Chapter 5

Imaging Flow Cytometry of Multi-Nuclearity

Ivan A. Vorobjev, Sultan Bekbayev, Adil Temirgaliyev, Madina Tlegenova, and Natasha S. Barteneva

Abstract

Multi-nuclearity is a common feature for cells in different cancers. Also, analysis of multi-nuclearity in cultured cells is widely used for evaluating the toxicity of different drugs. Multi-nuclear cells in cancer and under drug treatments form from aberrations in cell division and/or cytokinesis. These cells are a hallmark of cancer progression, and the abundance of multi-nucleated cells often correlates with poor prognosis.

The use of standard bright field or fluorescent microscopy to analyze multi-nuclearity at the quantitative level is laborious and can suffer from user bias. Automated slide-scanning microscopy can eliminate scorer bias and improve data collection. However, this method has limitations, such as insufficient visibility of multiple nuclei in the cells attached to the substrate at low magnification.

Since quantification of multi-nuclear cells using microscopic methods might be difficult, imaging flow cytometry (IFC) is a method of choice for this. We describe the experimental protocol for the preparation of the samples of multi-nucleated cells from the attached cultures and the algorithm for the analysis of these cells by IFC. Images of multi-nucleated cells obtained after mitotic arrest induced by taxol, as well as cells obtained after cytokinesis blockade by cytochalasin D treatment, can be acquired at a maximal resolution of IFC. We suggest two algorithms for the discrimination of single-nucleus and multi-nucleated cells. The advantages and disadvantages of IFC analysis of multi-nuclear cells in comparison with microscopy are discussed.

Key words Mitosis, Microtubule inhibitors, Cytochalasin D, Multi-nuclearity

1 Introduction

Cancer is related to genetic processes such as genome instability, rearrangements, or specific gene mutations, followed by epigenetic changes, which ultimately lead to deregulated cell proliferation. One of the specific features of cancer is the presence of multi-nucleated cells [1, 2]. In normal tissues, multi-nucleated cells of macrophage origin like foreign body giant cells, Langerhans' cells, and osteoclasts are present [3]. Besides, multi-nucleated cells of fibroblast origin are formed in some pathological processes

[4, 5]. The most interesting, however, is the formation and dynamics of multi-nucleated cells of cancer origin.

Multi-nucleation is observed in many cancers [6–8]. The abundance of polyploid multi-nucleated cells (MNCs) strongly correlates with resistance to chemotherapy [8, 9]. Dormant large multi-nucleated cells correlate with poor prognosis and are a hallmark of relapse after anticancer treatment (reviewed in [1, 2]). The frequency of the multi-nucleated cells in cancers increases after different chemotherapy treatments with taxanes [10, 11], doxorubicin [8, 9, 12], carboplatin [9, 13–15], and other drugs.

Polyploid multi-nucleated cancer cells can be generated by several mechanisms: (i) mitosis without cytokinesis resulting in the formation of plasmodium-like cell; (ii) cell-cell fusion with the formation of the syncytium, and (iii) through mitotic arrest followed by exit into the interphase without chromosome separation (mitotic slippage). The outcome of these processes is different. The first two mechanisms result in the formation of giant cells, with each nucleus of nearly normal size. In the last case, the nuclei formed are numerous and might be rather small since they contain one or few chromosomes [16]. These are called micronuclei. The technical challenge is whether one can distinguish such micronuclei from the lobulated ones formed by other processes [17] and also present in the cancer cell populations.

Currently, quantitative analysis of the multi-nucleated cells is hampered because of the limitations of manual assessment of the multi-nucleated cell frequency. Multi-nucleated cells containing micronuclei could be evaluated under the microscope only using relatively high magnification. This requires prolonged observations with 3D visualization; otherwise, results might be biased. The manual microscopy-based analysis is labor-intensive and time-consuming. Automated microscopy can partially eliminate this bias but suffers from the lack of image processing algorithms [18]. The task of cell nuclei counting is challenging due to the required nuclear segmentation of overlapping and/or touching nuclei and the presence of noise and image acquisition variables [19, 20]. Abnormalities in nuclei texture or shape are hallmarks of cancer cells, and highly textured nuclei fluorescent images can lead to apparent undesirable splitting of a single nucleus during image segmentation.

Of particular interest is the formation of multi-nucleated cells after mitotic arrest induced by anti-microtubule drugs frequently happening in cancer cells [21]. Microscopic evaluation of the frequency of mitotic slippage requires prolonged time-lapse recordings and manual data analysis of numerous time-lapse series [22–24]. Besides, many cells die soon after slippage [23, 25]. Thus, determining the outcome of mitotic arrest induced by drug treatments in cancer cells remains challenging.

Imaging flow cytometry (IFC) is a method of choice in the morphometric research of highly heterogeneous populations of cells [26]. IFC advantages are (1) imaging of single cells excluding a requirement of cellular segmentation and (2) high-throughput capabilities of instrumentation, allowing a standardized analysis of tenths to thousands of images based on morphological and fluorescent features.

Among the different types of nuclei, there are three nuclei types of particular interest: (1) lymphoid cell nuclei that are of regular shape and relatively small size; (2) epithelial cell nuclei with homogeneous, nearly uniform chromatin distribution; (3) nuclei of high-grade cancer cells that have irregular, pleomorphic boundaries, clear nucleoli and heterogeneous chromatin [27].

A detailed description of IFC application for the development of micronucleus assay using cells of lymphoid origin was given by Rodrigues and co-authors [18, 28], Verma and co-authors [29], and recently was expanded to skin epithelial cells [30]. The procedure of multi-nuclearity assessment might combine several basic image analysis algorithms such as watershed-based nuclei segmentation, thresholding, and intensity-based spot-counting. Watershed transform is one of the most popular approaches for nuclear and cellular image segmentation [31–33]. Spot-counting algorithms were intensively used for FISH and micronucleus image counting in gene toxicity and radiotoxicity research [34]. Machine-learning and deep learning approaches were developed recently for the analysis of complex label-free and immunofluorescent images where simple segmentation is not sufficient [35, 36].

Multi-nuclearity evaluation, as well as other nuclear morphometric and image features such as image texture, nucleus-to-cytoplasm ratio, nucleus size, pleomorphism degree, can be helpful in the evaluation of cancer grade and treatment efficiency [37]. Image analysis based on the texture parameters, i.e., radiomics and not on morphometry (length, area, size), remains challenging even after successful nuclear segmentation [38–40] and quantitation of cancer cells types due to the heterogeneous chromatin distribution in their nuclei still not possible. In the present study, we extend the IFC application for the analysis of attached cultured cancer cells with pleomorphic nuclei and show that promising results could be obtained by using the developed protocol.

Addressing the question about the feasibility of IFC to analyze the formation of multi-nucleated cells in cancer A549 cells (non-small lung cancer carcinoma), we tested two models – cytochalasin D-induced multi-nucleation and multi-nucleation after mitotic slippage under paclitaxel treatment after Hoechst 33342 staining. In the first model, the formation of multi-nucleated cells occurs through "endomitosis", i.e., mitosis without cytokinesis [41]. According to the microscopic analysis, these cells usually have 3–6 nuclei of the same size and form [42]. In the second

model, multi-nucleated cells are tetraploid ones that have formed after mitotic slippage [24]. These cells contain a different number of nuclei, including so-called micronuclei [43].

Galleries of multi-nucleated cells and cells with a single nucleus can be easily obtained (Fig. 1a and b) manually; however, many images come into the "gray" zone. The use of the EDF (extended depth of focus) function resulted in a significant enhancement of the contrast of the fluorescent images making the texture more evident but precluded visual analysis of multi-nuclearity.

The percentage of cells with more than one nucleus was further determined using machine-learning approaches. The standard approach to analyze multi-nuclearity described in detail by Rodriguez and others [18, 28] has limitations in the discrimination of mononucleated and multi-nucleated cells with pleomorphic nuclei because of the insufficient gradients at the nuclear edges. When EDF option was activated, nuclear staining became more heterogeneous, and also analysis by a complex of masks was inefficient. Since some of the multi-nucleated cells could be easily distinguished by manual visual inspection, we further employed a machine-learning algorithm. This protocol gave a good separation of the test galleries (Fig. 2a).

Statistical data were collected for both categories (single-nucleated and multi-nucleated) and were comparable with the results obtained by machine-learning algorithm (multi-classifier 2 at Fig. 2b). For the comparison we took a useful parameter that is cell diameter/area (cell volume). The area size of multi-nucleated taxol-treated cells was 118% from the single-nucleated taxol-treated cell population and the overlap between two distributions is larger than for the multi-classifier (Fig. 2c).

Manual inspection of image galleries obtained from control and taxol-treated cells using different cut-off values on the multi-classifier axis show that undoubtedly single nucleated cells are located on the multi-classifier histogram below −0.3, and undoubtedly multi-nucleated cells are located on the histogram above 0.5 (Fig. 3d and e). We suggest that a reasonable estimate of the minimal percentage of multi-nucleated cells with a high degree of heterogeneity in chromatin staining can be obtained using a machine-learning approach.

For a more detailed analysis of multi-nuclear cells, we used high-resolution confocal microscopy. Confocal microscopy taken with an equivalent pixel size of 70 nm in X-Y plane and step of 100 nm along the Z axis (LSM 780, PlanApo 63×/1.4 Oil immersion objective) shows complex morphology of nuclei in untreated cells (Fig. 3a) and gives a larger number of nuclei after treatments (Fig. 3b), but takes a lot of time for analysis of individual cells (scanning of one z-stack across the cell takes about 5–10 min) and does not allow evaluation of the frequency of multi-nucleated cells in the population. However, in some cases in the cells that have
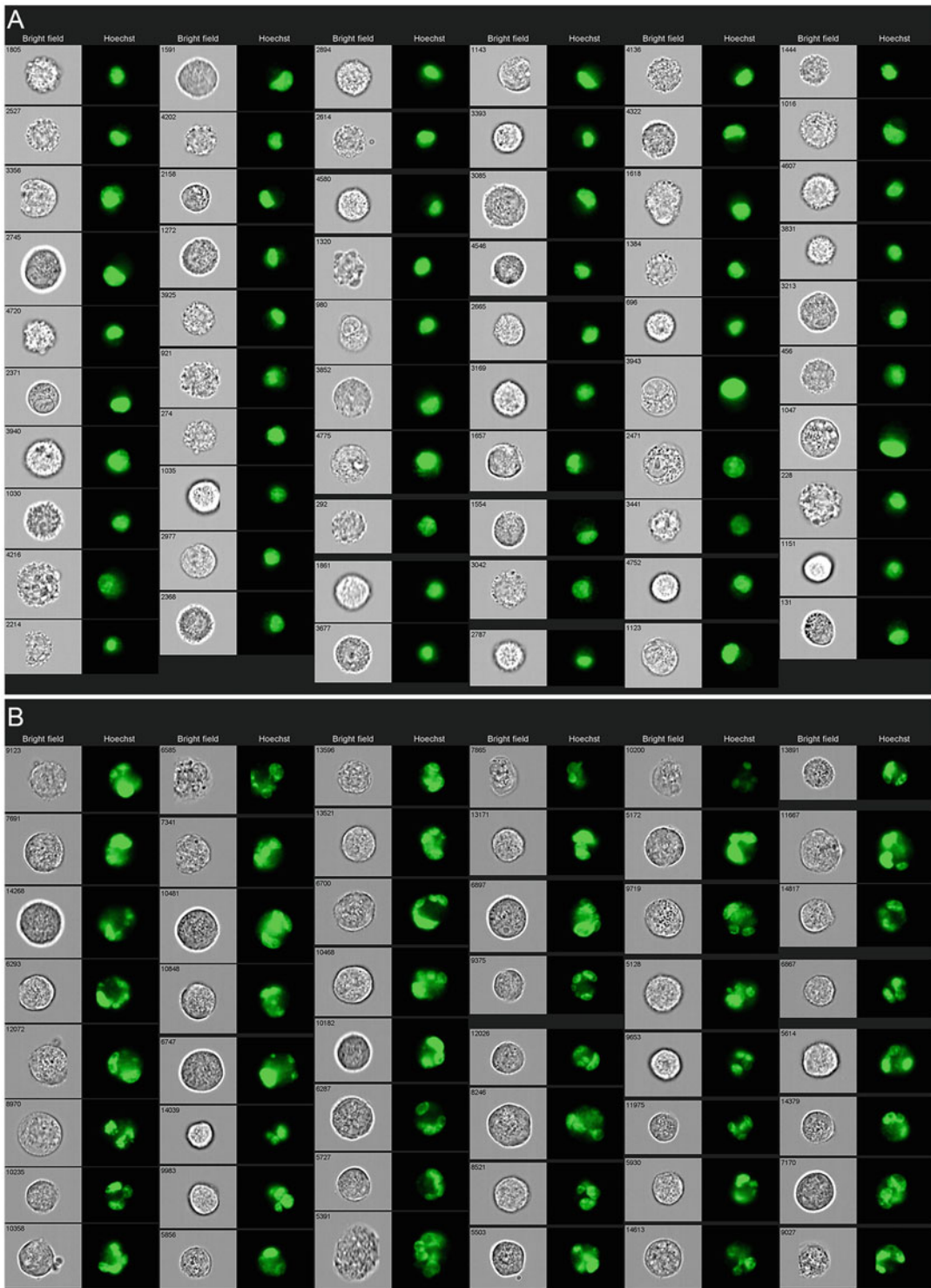
Fig. 1 (**a**) Mono-nucleated A549 cells. (**b**) Multinucleated A549 cells collected after mitotic slippage. The presence of multiple nuclei/nuclear lobes is evident, but discrimination between multilobularity (one nucleus with many lobes) and true multi-nuclearity (many nuclei) is not possible. Notice that the size difference between cells in (**a**) and (**b**) is negligible (Brightfield)

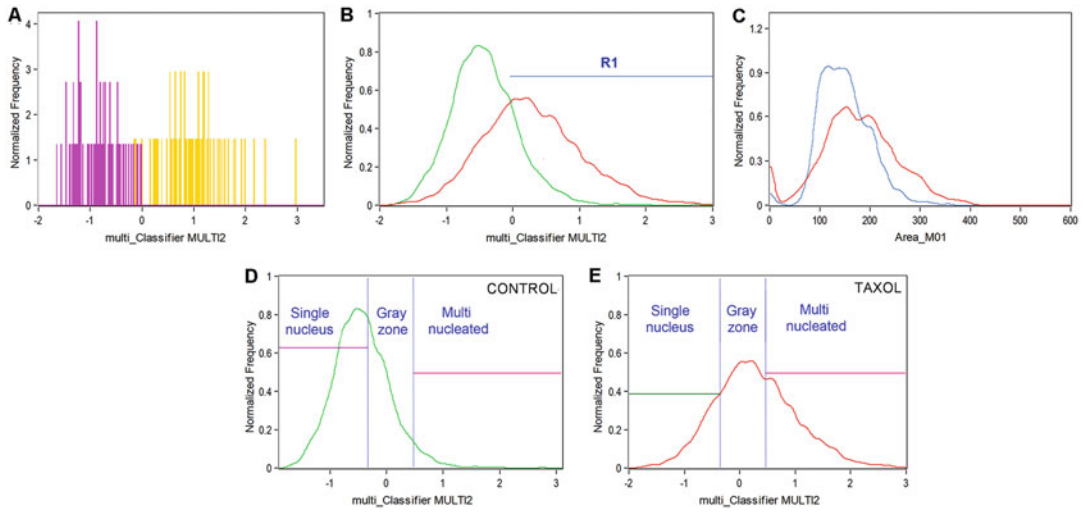**Fig. 2** (**a**) Histograms of mono- and multi-nucleated cells from training galleries for machine learning algorithm (purple- mono-nucleated and yellow – multi-nucleated cells). (**b**) Histograms of events distribution along Classifier Multi2. (Green – control A549 cells, red – A549 cells treated with taxol (analyzed with FlowJo (BD Biosciences, USA). R1 defines the region of multi-nucleated cells. (**c**) Histograms of Area parameter in control and treated with taxol A549 cells (128% of area) (blue – mono-nucleated cells; red- multi-nucleated cells). (**d-e**) Histograms of Control (Green) and Taxol-treated (Red) cellular populations distributed along multi-classifier 2. Gated mono-nucleated and multi-nucleated regions in each cell population, and Gray Zone (between −0.3 and 0.5 scores) where identification of multi-nuclearity is ambiguous.
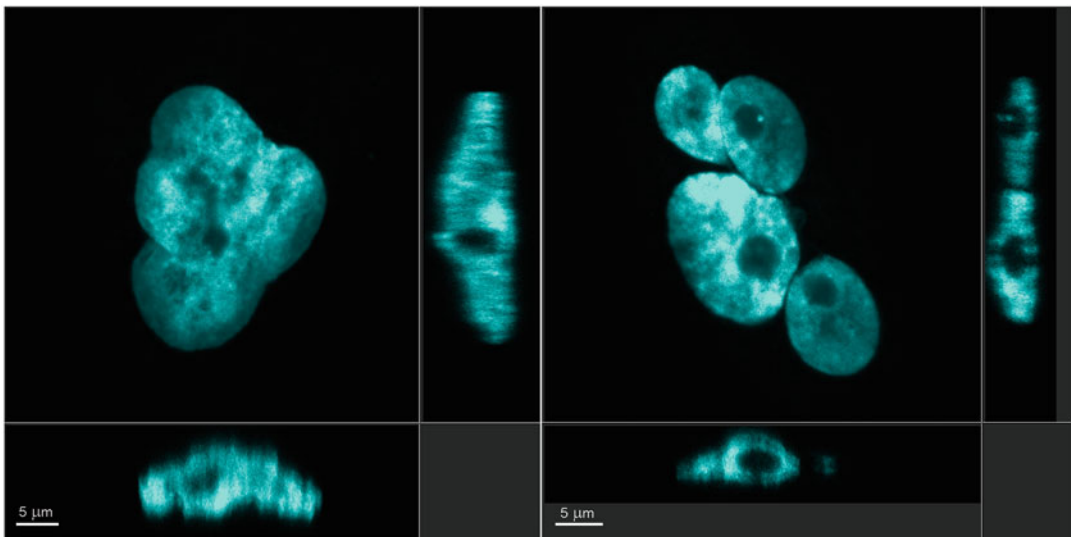

Fig. 3 Laser scanning confocal images of mono-nucleated multi-lobular (**a**) and multi-nucleated (**b**) cells in culture. X-Y projection is given on the right; X-Z projection is given on the left, Y-Z projection is given at the bottom. Hoechst 33342 staining. Scale bar 5 microns

formed after mitotic slippage, exact discrimination of multiple nuclei from each other is not possible even by microscopy. Thus, the detailed analysis of the multi-nuclearity complex approach - IFC for the frequency of multi-nucleated cells and confocal microscopy for the estimation of the average number of nuclei per cell - is recommended.

We conclude that though IFC is limited in recognition of multiple micronuclei from the multi-lobed mononuclear cancer cells with pleomorphic nuclei, it stays the best method to determine the frequency of multi-nucleated cancer cells.

2 Materials

2.1 Laboratory Instrumentation and Accessories

1. Imagestream X MKII (Amnis-Luminex, USA) 4-lasers system with 60× magnification.

2. Laser scanning confocal microscope (LSM-780, Zeiss, Germany).

3. Centrifuge without refrigeration (Eppendorf Centrifuge 5702, USA).

4. Light inverted microscope (Zeiss Primovert, Germany).

5. Motorized inverted fluorescent microscope (Zeiss Cell Observer, Germany).

6. Thermoblock (Thermo Fisher Scientific 3121 Water-Jacketed CO_2 Incubator with IR Sensor, USA).

7. Standard laminar flow hood (Thermo Fisher Scientific, USA).

8. Standard hemocytometer.

9. Sterile cultural ventilated flasks (25 cm^2) and multi-well plates (TPP, Switzerland).

10. 15 ml centrifugation tubes (TPP, Switzerland).

11. Petri dishes with a glass-bottom (Corning, USA).

2.2 Reagents

1. Complete DMEM medium: DMEM supplemented with L-glutamine, Pen-Strep (penicillin-streptavidin), and 5% fetal bovine serum (FBS).

2. CO_2-independent DMEM medium (Gibco™, ThermoFisher 18045088, USA).

3. 0.5% CO_2-independent DMEM media with 1% FBS (DMEM with 1% FBS was diluted 1:1 by distilled water). For this, 25 mL of sterile distilled water was mixed thoroughly with 25 mL CO_2-independent medium in laminar-flow hood. 500 µL was removed from this solution, and 500 µL of FBS was added and mixed thoroughly.

4. Fetal Bovine Serum (Sigma F2442, USA, sterile-filtered, suitable for hybridoma).

5. DMEM media, penicillin, streptomycin, L-glutamine suitable for cell culture.

6. Hoechst 33342.

7. Taxol (Paclitaxel, Sigma T7402, USA).

8. Cytochalasin D.

9. Trypsin-EDTA 0.25% sterile solution.

10. Phosphate buffered saline.

3   Methods

3.1   Cancer Cell Line A549 Culturing

1. Grow A549 cancer cell line in DMEM complete culture medium supplemented with L-glutamine, Pen-Strep. and 5% FBS in 25 cm^2 culture flasks or multi-well plates (6-well plates (TPP, Switzerland)).

3.2   Growing A549 Cellular Monolayer with Taxol

1. After cells reach a subconfluent density, add Taxol (Sigma, USA) to the final concentration of 100 or 300 ng/mL (100–300 nM) and leave for 24 h in the CO_2 incubator.

2. After 24 h, remove the Taxol by changing the culture medium.

3. Wash a monolayer with 5 ml of the culture medium and gently shake the flask.

4. Transfer cultural medium with detached mitotic cells into a 15 mL tube.

5. Centrifuge mitotic cells in cell centrifuge at 300 g for 3 min.

6. After centrifugation, dispose a supernatant and collect pellet in 7 mL of complete DMEM with 5% FBS.

7. Centrifuge cell suspension again in fresh culture medium at 300 g for 3 min.

8. Dispose supernatant again, resuspend a pellet carefully in 7 ml of a complete DMEM, and seed cells in a new Petri dish (*see* **Note 1**).

9. Incubate cells in a Petri dish in a drug-free medium in CO_2 incubator at 37 °C and 5% CO_2 for 12 h.

3.3   Growing A549 Cellular Monolayer with Cytochalasin D

1. After cells reach a subconfluent density in multi-well plates add Cytochalasin D (Sigma, USA) to a final concentration of 0.5 μM and culture cells with the drug for 72 h.

2. After three days of incubation, remove the drug by replacing three times the culture medium with drug-free complete DMEM with 5% FBS.

3. Incubate cells in a drug-free medium in CO_2 incubator at 37 °C and 5% CO_2 for another 24 h.

3.4 Preparation of Multi-Nucleated Cellular Suspension after Taxol or Cytochalasin D Treatment for Analysis on Imagestream X Mark II

1. After 12 h of post-Taxol growing of A549 cellular monolayer in Petri dish, rinse cells three times with 3 mL 1× PBS.

2. Then rinse cellular monolayer two times with 2 mL solution of 0.05% Trypsin with 0.5 mM EDTA (in PBS).

3. Incubate cells in a Petri dish in 1 mL solution of Trypsin (0.05%) with 0.5 mM EDTA for 3 min (*see* **Note 2**).

4. After detach cells from the dish surface, add 5 mL DMEM with 5% FBS, resuspend cells, and collect in 15 mL centrifuge tube.

5. Take 10 μL of cell suspension and count cells with a standard hemocytometer or automatic hemocytometer Countess 3 (Thermo Fisher Scientific, USA).

6. Prepare cellular suspension containing 500,000 cells and centrifuge at 300 g for 3 min.

7. After centrifugation, dispose a supernatant and resuspend a cellular pellet in 2 mL of hypotonic (0.5×) CO_2-independent medium containing 1% FBS with 5.5 μM Hoechst 33342.

8. Transfer cell suspension in the Eppendorf tube and incubate in a thermostat at 37 °C for 30 min with periodical agitation every 5 min.

9. At the end of the incubation centrifuge a cellular suspension in Eppendorf centrifuge at 300 g for 3 min.

10. Dispose the major part of the supernatant, and resuspend pellet collecting 100,000–500,000 cells in approximately 60 μL of remaining supernatant.

3.5 Analysis of Micronuclei in Multi-Nucleated Cells under Microscope

1. Seed a cellular suspension of A549 cell line after treatment with Taxol for 24 h and subsequential drug removal in 3.5 cm Petri dishes with a glass bottom (Corning, USA).

2. Incubate cells in a Petri dish in CO_2-incubator 12 h at 37 °C 5% CO_2.

3. After 12 h of incubation, dispose cultural medium and rinse cells with 2 mL 1× PBS pre-warmed up to 37 °C.

4. Add 2 mL of 1% glutaraldehyde solution in 1× PBS to the cells and incubate for 30–60 min (*see* **Note 3**).

5. Remove a glutaraldehyde solution from a Petri dish.

6. Rinse cell monolayer in the Petri dish with 1×PBS for 30 min by changing 1×PBS three times every 10 min.

7. Add 1× PBS containing 5.5 μM Hoechst 33342 to a Petri dish for at least for 30 min (*see* **Note 4**).

8. Take images using Zeiss Axio Observer microscope (Zeiss, Germany) equipped with 63×/1.46 oil immersion objective and Hamamatsu ORCA-FLASH II camera in DIC and DAPI channels as 5×5 tiles with z-stack (15 μm size using 0.3 μm step).

9. Deconvolve z-stacks using Huygens software (Scientific Volume Imaging, Netherlands) and count nuclei manually.

3.6 Preparation Cells for Imaging Flow Cytometry Analysis

1. Seed A549 cells line after treatment with Taxol for 24 h and drug removal into 3.5 cm Petri dishes (Corning, USA).

2. Incubate cells in a Petri dish in CO_2-incubator for 12 h at 37 °C 5% CO_2.

3. After 12 h incubation of taxol-treated cells in the drug-free medium, dispose culture medium and rinse cells 3 times with 3 mL of PBS.

4. Then rinse cells 2 times with 2 mL Trypsin 0.05% with 0.5 mM EDTA, and incubate in 1 mL Trypsin (0.05%) with 0.5 mM EDTA for 3 min.

5. After cells detach from the surface, add 5 mL DMEM with 5% FBS, resuspend cells, and collect in 15 mL tube (*see* **Note 5**).

6. Dispose the supernatant and resuspend the pellet of cells in 2 mL hypotonic (0.5×) CO_2-independent medium containing 1% FBS with 5.5 μM Hoechst 33342 (*see* **Note 6**).

7. After incubation in hypotonic medium for 10 min., sediment the cells by centrifugation at 300 g for 3 min.

8. Dispose the major part of the supernatant cautiously and resuspend the pellet in 60–100 μL of the same medium (*see* **Note 7**).

3.7 Starting and Running Imagestream X Mark II

1. Fill out instrument sheath and cleaning containers (cleanser, debubbler, sterilizer), empty waste, and check the speed beads container. Load **Default Template** from **File** Menu. Run all required calibrations and tests (*see* **Note 8**).

2. Select magnification at 60×, and high sensitivity mode. Turn on and optimize power of 405 nm (and 488 nm, if required) lasers. Disable other lasers (see **Note 9**).

3. Select the **Scatterplot** icon. Then select Area M01 on the X-axis and Aspect Ratio M1 on the Y-axis. Draw the region around single cells.

4. Set the acquisition parameters, specify the file name and the destination folder, and change the events number to 10,000-20,000. Collect bright-field imagery in channels 1 and 9, and side scatter in channel 6, minimizing signal and avoiding saturation.

5. Click on **Load** and apply an Eppendorf tube with sample in the sample port when prompted to do so.

6. Acquire 10,000–20,000 cellular events. Define nuclear events as positive for staining with Hoechst 33342. Create a histogram using as a parameter **Intensity M07** and draw a region defining cellular events positive for Hoechst 33342.

7. Launch the IDEAS software analysis package. Spectral compensation is not required unless additional staining is involved. Open the file in the IDEAS software.

8. Create analysis template for the identification of single events using dotplot with parameters **Area M01** on the X-axis and **Aspect Ratio M1** on the Y-axis, and create a region around single cells, and name it **Single Cells**.

9. Create a dotplot with Gradient **RMS M01** on the X-axis, and Gradient **RMS M07** on the Y-axis. Select **Single Cells** as a parent population. Draw the region and name it **Focused Cells**.

10. Create two galleries with manually picked cells with clearly identifiable single individual nuclei (Fig. 1) and with multi-nucleated cells (> 30 cells each).

3.8 Evaluation of Multi-Nuclear Cells Using Machine-Learning Module

In this protocol, a machine-learning module of "IDEAS" vs. 6.3 software (Amnis-Luminex, USA) is used.

1. After creating training galleries of images, start machine-learning Module to create a new parameter for image analysis.

2. Choose populations (single, focused) if the populations are **GATED** or **ALL** if they are not gated.

3. After populations of interest have been tagged, and galleries of images were chosen, use control-click to select training galleries (single and multi-nucleated cells). Alternatively, use the tagging tool to create galleries (*see* **Note 11**).

4. To exclude existing irrelevant features from different categories during step 3, select categories that best discriminate your data (*see* **Note 12**).

5. Choose channels to analyze the images (Channel 7 – Hoechst 33343 staining).

6. Click the "Start" button to create a single multi-parameter, and verify its content.

7. After creating the classifier, you can **Edit** or **Finish** and exit the wizard.

8. View new multi-classifier features in the feature manager. Click on the Analysis tab and select a new feature created and see the weight of different components in the new Feature.

9. Apply a new multi-component classifier to the populations of interest. For example, multi-classifier 1 (a combination of Mean and Min Pixel and Lobe Count features that uses Morphology and Skeleton Masks for Channel 7 (Hoechst 33343); multi-feature classifier 2 (a combination of Bright Detail Intensity and Variance Mean that uses fluorescent mask from Channel 7).

10. Create histograms from merged file to compare control and taxol-treated samples using a new chosen multi-feature.

11. Export FCS information from a file and analyze it using FlowJo (Treestar-BD Biosciences, USA) or FACSExpress (De Novo software, USA) off-line analysis program. Apply the Kolmogorov-Smirnov test to verify whether differences between overlapping histograms are significant (Fig. 2b).

4   Notes

1. If the multi-nucleated cells will be observed with a microscope, use glass-bottom Petri dishes (Corning, USA).

2. Time needed for the complete detachment of cells might vary. Incubation should be ended when a majority of cells start rolling on the surface of the flask.

3. Cells could be fixed with PFA; however, it will result in slight shrinkage of cells making analysis of the multi-nuclearity more difficult.

4. Images could be taken with laser scanning confocal microscope; however, this method is laborious and not useful for quantification of the proportion of multi-nucleated cells in the cellular population. This stage is important for the 3D reconstruction and determining the true number of micronuclei per cell, but not for the enumeration of the proportion of multi-nucleated cells.

5. This stage is important for the 3D reconstruction and for determining the number of micronuclei per cell, but not for the enumeration of multi-nucleated cells.

6. At this stage, 10 μL of suspension should be taken, and number of cells should be counted on a hemacytometer. Whether the overall concentration of cells exceeds 1 mln/ml, you can continue in the way described below. When concentration of cells is lower, you should cautiously collect cells after each step. When the concentration of cells is below 500,000 per ml, the number of cells after the end of specimen preparation could be low, and this will slow down ImageStream-based acquisition even when cells will be resuspended in the minimal volume.

7. Cell suspension in the Eppendorf tube should be agitated every 5–7 min and incubated in 37 °C for 30 min.

8. If the concentration of cells after first sedimentation (step 5) was low (less than 1 mln/mL), the volume for resuspension should be minimal – about 40–50 μL.

9. When you click "Startup" button make sure that the checkbox for Start all calibrations and tests is checked. It will calibrate the instrument following the start up.

10. Make sure that all cells can be seen in the Cell View column and that debris is excluded from viewing and acquisition (use the Single Cell gating for this purpose). Exclude the images with saturated pixels by changing the excitation laser powers.

11. The IDEAS software (Amnis-Luminex, USA) machine-learning module requires at least 25 images to be included in the training galleries. We recommend 40–50 images if it is possible. Unobvious and/or controversial images should not be included into training galleries. More than two galleries can be created and used.

12. Try to exclude different categories or some features irrelevant to the task during step 3 of creating multi-parameter classifier.

Acknowledgments

References

1. Mirzayans R, Andrais B, Murray D (2018) Roles of polyploid/multinucleated giant cancer cells in metastasis and disease relapse following anticancer treatment. Cancers 10:118–129. https://doi.org/10.3390/cancers10040118

2. Mirzayans R, Murray D (2020) Intratumor heterogeneity and therapy resistance: contributions of dormancy, apoptosis reversal (anastasis) and cell fusion to disease recurrence. Int J Mol Sci 21:1308. https://doi.org/10.3390/ijms21041308

3. Anderson JM (2000) Multinucleated giant cells. Curr Opin Hematol 7:40–47. https://doi.org/10.1097/00062752-200001000-00008

4. Regezi JA, Courtney RM, Kerr DA (1975) Fibrous lesions of the skin and mucous membranes which contain stellate and multinucleated cells. Oral Surg Oral Med and Oral Pathol 39:605–614

5. Cho MI, Garant PR (1984) Formation of multinucleated fibroblasts in the periodontal ligaments of old mice. Anat Rec 208:185–196

6. Fishback NF, Travis WD, Moran C, Guinee D Jr, McCarthy W, Koss M (1994) Pleomorphic (spindle/giant cell) carcinoma of the lung. Cancer 73:2936–2945

7. Ryska A, Reynolds C, Keeney GL (2001) Benign tumors of the breast with multinucleated stromal giant cells. Immunohistochemical analysis of six cases and review of the literature. Virchows Arch 439:768–775. https://doi.org/10.1007/s004280100470

8. Parekh A, Das S, Parida S, Das CK, Dutta D, Mallick SK (2018) Multi-nucleated cells use ROS to induce breast cancer chemo-resistance in vitro and in vivo. Oncogene 37:4546–4561. https://doi.org/10.1038/s41388-018-0272-6

9. Rohnalter V, Roth K, Finkernagel F, Adhikary T, Obert J, Dorzweiler K et al (2015) A multi-stage process including

transient polyploidization and EMT precedes the emergence of chemoresistent ovarian carcinoma cells with a dedifferentiated and proinflammatory secretory phenotype. Oncotarget 6:40005–40025. https://doi.org/10.18632/oncotarget.5552

10. Kadota K, Suzuki K, Colovos C, Sima CS, Rusch VW, Travis WD, Adusumilli PS (2012) A nuclear grading system is a strong predictor of survival in epitheloid diffuse malignant pleural mesothelioma. Mod Pathol 25:260–271. https://doi.org/10.1038/modpathol.2011.146

11. Ogdena A, Ridaa PCG, Knudsenb B, Kucukc O, Anejaa R (2015) Docetaxel-induced polyploidization may underlie chemoresistance and disease relapse. Cancer Lett 367:89–92. https://doi.org/10.1016/j.canlet.2015.06.025

12. Weihua Z, Lin Q, Ramoth AJ, Fan D, Fidler IJ (2011) Formation of solid tumors by a single multinucleated cancer cell. Cancer 117:4092–4099. https://doi.org/10.1002/cncr.26021

13. Bagnyukova TV, Serebriiskii IG, Zhou Y, Hopper-Borge EA, Golemis EA, Astasturov I (2010) Chemotherapy and signaling: how can targeted therapies supercharge cytotoxic agents? Cancer Biol Ther 10:839–853. https://doi.org/10.4161/cbt.10.9.13738

14. Kuo CH, Lu YC, Tseng YS, Shi CS, Chen SH, Chen PT, Wu FL, Chang YP, Lee YR (2014) Reversine induces cell cycle arrest, polyploidy, and apoptosis in human breast cancer cells. Breast Cancer 21:358–369. https://doi.org/10.1007/s12282-012-0400-

15. Lu YC, Lee YR, Liao JD, Lin CY, Chen YY, Chen PT et al (2016) Reversine induced multinucleated cells, cell apoptosis and autophagy in human non-small cell lung cancer cells. PLoS One 11:e0158587. https://doi.org/10.1371/journal.pone.0158587

16. Zhu Y, Zhou Y, Shi J (2014) Post-slippage multinucleation renders cytotoxic variation in anti-mitotic drugs that target the microtubules or mitotic spindle. Cell Cycle 13:1756–1764. https://doi.org/10.4161/cc.28672

17. Nakayama Y, Yamaguchi N (2005) Multi-lobulation of the nucleus in prolonged S phase by nuclear expression of Chk tyrosine kinase. Exp Cell Res 304:570–581. https://doi.org/10.1016/j.yexcr.2004.11.027

18. Rodrigues MA (2018) Automation of the in vitro micronucleus assay using the Image-Stream imaging flow cytometer. Cytometry A 93A:706–726. https://doi.org/10.1002/cyto.a.23493

19. Coelho LP, Shariff A, Murhy RF (2009) Nuclear segmentation in microscope cell images: a hand-segmented dataset and comparison of algorithms. In: IEEE international symposium on biomedical imaging: from Nano to macro. ISBI'09. IEEE, pp 518–521

20. Xing F, Yang L (2013) Robust nucleus/cell detection and segmentation in digital pathology and microscopy images: a comprehensive review. IEEE Rev Biomed Engineer 9:234–263

21. Gascoigne KE, Taylor SS (2009) How do anti-mitotic drugs kill cancer cells? J Cell Sci 122:2579–2585. https://doi.org/10.1242/jcs.039719

22. Gascoigne KE, Taylor SS (2008) Cancer cells display profound intra- and interline variation following prolonged exposure to antimitotic drugs. Cancer Cell 14:111–122. https://doi.org/10.1016/j.ccr.2008.07.002

23. Orth JD, Kohler RH, Foijer F, Sorger PK, Weissleder R, Mitchison TJ (2011) Analysis of mitosis and antimitotic drug responses in tumors by in vivo microscopy and single-cell pharmacodynamics. Cancer Res 71:4608–4616. https://doi.org/10.1158/0008-5472.CAN-11-0412

24. Cheng B, Crasta K (2017) Consequences of mitotic slippage for antimicrotubule drug therapy. Endocr Relat Cancer 24:T97–T106. https://doi.org/10.1530/ERC-17-0147

25. Shi J, Orth JD, Mitchison T (2008) Cell type variation in responses to antimitotic drugs that target microtubules and kinesin-5. Cancer Res 68:3269–3276

26. Barteneva N, Vorobjev IA (2018) Cellular heterogeneity: methods and protocols. Met Mol Bio 1745. https://doi.org/10.1007/978-1-4939-7680-56

27. Irshad H, Veillard A, Roux L, Racoceanu D (2014) Methods for nuclei detection, segmentation and classification in digital histopathology: a review-current status and futire potential. IEEE Rev Biomed Engineering 7:97–114

28. Rodrigues MA, Beaton-Green LA, Kutzner BC, Wilkins RC (2014) Automated analysis of the cytokinesis-block micronucleus assay for radiation biodosimetry using imaging flow cytometry. Radiat Environ Biophys 53:273–282. https://doi.org/10.1007/s00411-014-0525-x

29. Verma JR, Harte DSG, Shah U-K, Summers H, Thornton CA et al (2018) Investigating Flow-Sight imaging flow cytometry as a platform to assess chemically induced micronuclei using human lymphoblastoid cells in vitro.

Mutagenesis 33:283–289. https://doi.org/10.1093/mutage/gey021

30. Allemang A, Thacker R, DeMarco RA, Rodrigues MA, Pfuhler S (2021) The 3D reconstructed skin micronucleus assay using imaging flow cytometry and deep learning: proof-of-principle investigation. Mutation Res Gen Toxicol Environment Mutagenesis 865: 503314. https://doi.org/10.1016/j.mrgentox.2021.503314

31. Cheng J, Rajapakse JC (2008) Segmentation of clustered nuclei with shape markers and marking function. IEEE Transact Biomed Engineering 56:741–748. https://doi.org/10.1109/TBME.2008.2008635

32. Phansalkar N, More S, Sabale A, Joshi M (2011) Adaptive local thresholding for detection of nuclei in diversity stained cytology images. Proc Int Conf Communications and Signal Processing, In, pp 218–220. https://doi.org/10.1109/ICCSP.2011.5739305

33. Meijering E (2012) Cell segmentation: 50 years down the road. IEEE Signal Process Mag 29:140–145

34. Hernandez L, Terradas M, Martin M, Tusell L, Genesca A (2013) Highly sensitive automated method for DNA damage assessment: gamma-H2AX foci counting and cell cycle sorting. Int J Mol Sci 14:15810–15826. https://doi.org/10.3390/ijms140815810

35. Lippeveld M, Knill C, Ladlow E, Fuller A, Michaelis LJ et al (2020) Classification of human white blood cells using machine learning for stain-free imaging flow cytometry. Cytometry 97A:308–319. https://doi.org/10.1002/cyto.a.23920

36. Phillip JM, Han K-S, Chen W-C, Wirtz D, Wu P-H (2021) A robust unsupervised machine learning method to quantify the morphological heterogeneity of cells and nuclei. Nat Protocols 16:754–774. https://doi.org/10.1038/s41596-020-00432-x

37. Kumar N (2017) A dataset and a technique for generalized nuclear segmentation for computational pathology. IEEE Transact Med Imaging 36:1550–1560

38. Thibault G, Fertil B, Navarro C, Pereira S, Cau P, Levy N, Sequeira J, Mari J-L (2013) Shape and textures indexes application to cell nuclei classification. Inter J Pattern Recogn 27:1357002–1357025. https://doi.org/10.1142/S0218001413570024

39. Thibault G, Angulo J, Meyer F (2017) Advanced statistical matrices for texture chracterization application to cell nuclei classification. IEEE Transact Biomed Engineering 61:630–637. https://doi.org/10.1109/TBME.2013.2284600

40. Lee H-K, Kim C-H, Bhattacharjee S, Park H-G, Prakash D, Choi H-K (2021) A paradigm shift in nuclear chromatin interpretation: from qualitative intuitive recognition to quantitative texture analysis of breast cancer cell nuclei. Cytometry A 99A:698–706. https://doi.org/10.1002/cyto.a.24260

41. Klisch K, Pfarrer C, Schuler G, Hoffmann B, Leiser R (1999) Tripolar acytokinetic mitosis and formation of feto-maternal syncitia in the bovine placentome: different modes of the generation of multi-nuclear cells. Anat Embryol 200:229–237. https://doi.org/10.1007/s004290050275

42. Copeland M (1974) The cellular response to cytochalasin B: a critical overview. Cytologia 39:709–727

43. Riffell JL, Zimmerman C, Khong A, McHardy LM, Roberge M (2009) Effects of chemical manipulation of mitotic arrest and slippage on cancer cell survival and proliferation. Cell Cycle 8:3029–3042. https://doi.org/10.4161/cc.8.18.9623